CFD study on electrolyte distribution in redox flow batteries



2015 J. Phys.: Conf. Ser. 655 012049

(http://iopscience.iop.org/1742-6596/655/1/012049)

Journal of Physics: Conference Series **655** (2015) 012049 doi:10.1088/1742-6596/655/1/012049

# CFD study on electrolyte distribution in redox flow batteries

**S Bortolin**[1], **P Toninelli, D Maggiolo**, **M Guarnieri and D Del Col**

[1] Corresponding Author: stefano.bortolin@unipd.it

Università degli Studi di Padova, Dipartimento di Ingegneria Industriale
Via Venezia 1, 35131- Padova

**Abstract.** The most important component in a redox flow battery (RFB) cell is the MEA (membrane electrode assembly), a sandwich consisting of two catalyzed electrodes with an interposed polymeric membrane. In order to allow electrolyte flow toward the electroactive sites, the electrodes have a porous structure that can be obtained with carbon base materials such as carbon felts. The RFB cell is closed by two plates containing the distribution flow channels. Considering that a uniform electrolyte distribution in the reaction region is a prerequisite for high-efficiency operation, the flow pattern is an important parameter to be investigated for the optimization of the cell.
In the present work, the effect of different channels patterns on the electrolyte distribution and on the pressure drop is numerically investigated. Three-dimensional simulations have been carried out with ANSYS Fluent code and four different layouts have been considered. Calculations have been performed both in the distribution channels and in the felt porous region.

## 1. Introduction

The recent attention to environmental problems has led to an increasing use of renewable sources. However, the intermittent nature of most renewable energy sources has posed a serious challenge for widespread application and for an effective replacement of conventional sources. Therefore, energy storage plays a crucial role in the delivery of electricity from renewable sources, such as solar and wind, providing a solution for the balance problem between the generation and the consumption of the electric power. Nowadays, several energy storage technologies, characterized by different levels of development, have been proposed (e.g. pumped hydro, electrochemical, thermal, compressed air, flywheel...) as reviewed by Alotto *et al.* [1]. Among electrochemical systems, redox flow batteries (RFBs) represent one of the most recent technologies and a highly promising choice for stationary energy storage. Unlike conventional batteries, in which energy is stored in the battery structure, redox flow batteries store energy in two solutions containing different redox couples with proper electrochemical potentials. The electrolyte is stored in two separated tanks. The most appealing features of this technology are: scalability and flexibility, independent sizing of power and energy, long durability, fast responsiveness, and reduced environmental impact. Such features allow for wide ranges of operational power and discharge time, making RFBs an ideal solution for assisting electricity generation from renewable sources. The power size depends on the flow rate of electrolyte and the configuration of the cell stack, whereas the energy stored depends on the reactants chosen, their concentration and the size of the reactant tanks.
The main element of RFB is the membrane-electrode assembly (MEA) where the reduction and oxidation reactions take place in two liquid electrolytes (aqueous and not-aqueous) that contain a

given concentration of metal ions (the active material). The MEA is composed by two catalyzed electrodes (porous media such as carbon felt or metallic foam) with an interposed polymeric membrane. Finally, the RFB is closed by two plates containing the frame flow that can have different configurations to guarantee the best electrolyte distribution inside the porous media. During the charge/discharge operations, the electrons obtained from the redox reactions are collected by one electrode and go to the other one through an external circuit, whereas the ions migrate through the membrane. As compared to the conventional electrochemical batteries, the electrolytes are not permanently sealed, but they are stored in tanks and pumped into the cell stack. Furthermore, if the material of the two electrolytes is the same, as in the case of the vanadium redox flow batteries, then the cross-contamination problem during operation is limited. For these two aspects, the electrolytes have no degradation and a long life of RFB is guaranteed and can be also improved by its configuration, i.e. number of tanks, regulation of flow, type of electrolytes, electrodes, membrane and so on, as analyzed by Cunha *et al.* [2]. The RFB can be categorized by the active species or solvent (aqueous and non-aqueous, respectively), as reported in detail by Weber *et al.* [3] and Ponce de León and coworkers [4].
There are three important aspects related to RFBs design:

- the dimension of whole plant: it is pretty large making their use difficult for a mobile application, as reported by Cunha *et al.* [2];
- the electrolyte temperature in the RFB: it can be controlled through the flow rate avoiding the solution precipitation that occurs outside the allowed operating temperature ranges. For example, a numerical investigation on temperature field inside the MEA has been performed by Wei *et al.* [5];
- the flow field design to achieve uniform distribution of the electrolyte with low pressure drop, minimizing the mass transfer polarization and avoiding problems about solubility limits, as analyzed by Weber *et al.* [3], Xu *et al.* [6] and Wei *et al.* [5].

This paper aims at analyzing the flow field inside the MEA where the electrochemical reactions take place. As mentioned above, the RFB performance is strictly influenced by the electrolyte distribution inside the carbon felt: it is important to investigate the best electrolyte distribution avoiding high pressure drop and stagnation zones inside the porous region. In the following sections, the geometry of different distribution layouts, the setting of CFD simulations and, finally, the results are reported in detail to evaluate the best configuration.

## 2. Geometry

In the scientific literature, different configurations have been proposed for the distribution of the electrolyte inside the porous felt where electrochemical reactions take place. In particular, two types of solutions can be found: with the first method (indirect feeding), the felt is fed by channels machined in the containing plates of the cell (e.g. parallel channels, serpentine channels), whereas the second solution consists of direct feeding the felt without the use of channels.
In the present work, the authors have focused their attention on four possible geometrical configurations (table 1), with the aim to improve the electrolyte distribution and to evaluate the pressure drop inside the RFB cell. For all the configurations, the geometry of the carbon felt is the same (length 260 mm, width 160 mm, depth 4.3 mm), beside the number and the hydraulic diameter (h.d.) of the square channels is varied. The first three configurations reported in table 1 are referred, as mentioned above, to the indirect feeding: the electrolyte enters the parallel square channels placed above the carbon felt (figure 1, case with 5 inlet parallel channels), then it is sent through the porous zone and it finally exits from the outlet channels (figure 1, case with 6 outlet channels). Instead, in the last configuration, the felt is directly fed with the electrolyte.

**Table 1.** Selected configurations for the distribution of the electrolyte.

| Configuration | Feeding | Hydraulic diameter [mm] | Number inlet channels | Number outlet channels |
|---|---|---|---|---|
| **1** | Indirect | 1 | 5 | 6 |
| **2** | Indirect | 2 | 5 | 6 |
| **3** | Indirect | 2 | 4 | 4 |
| **4** | Direct | 1 | 5 | 6 |

The four selected configurations reported in table 1 are used to analyze the influence of the following geometrical parameters on the electrolyte distribution inside the carbon felt:

- hydraulic diameter of the square channels forming the frame flow inside the MEA;
- number of inlet/outlet channels and their position on the carbon felt;
- direct/indirect feeding of electrolyte inside the porous zone.

*2.1. Mesh*

For all the configurations, a tridimensional domain with a structured mesh has been considered. For the purpose of computational time savings, the mesh is finer for regions near the channels walls and in the contact zone between the felt and the channels, whereas it is much coarser in the rest of the volume. In the case of the first three configurations, the mesh is composed of about 7.0 ÷ 7.6 $10^6$ hexahedral cells while, for the last configuration, the mesh is composed of about 5.7 $10^6$ elements. Furthermore, a mesh independence test has been performed for the first case. A new structured mesh composed of about 3.7 $10^6$ elements has been designed. The maximum deviation between the velocity field obtained with the two different meshes is about 1%.

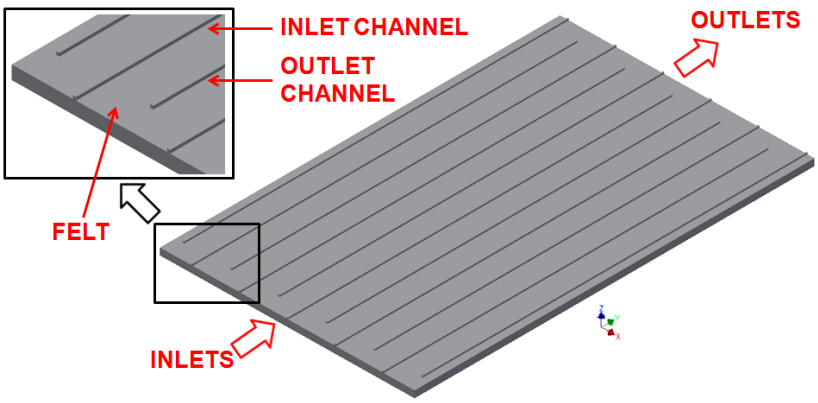


**Figure 1.** The carbon felt with distribution channels (configuration 1).

## 3. Numerical Methods

Three-dimensional and steady-state numerical simulations have been performed with ANSYS Fluent 15. The working fluid is a sulfuric acid water solution in which vanadium oxides are dissolved. The fluid is considered incompressible and its density and dynamic viscosity are, respectively, equal to 1354 kg $m^{-3}$ and 0.006 Pa s, as reported by Blanc and Rufer [7] and Tang *et al.* [8].

In all the simulations, the velocity inlet condition has been calculated from an estimation of the cell volumetric flow rate $Q_{cell}$ that was considered to be the same for all the studied cases. The evaluation of volumetric flow rate has been performed at fixed operational conditions of the RFB, as reported in equation (1):

$$Q_{cell} = n_m n_{ch} A_{ch} v_{in} = \frac{J A_m \alpha_Q}{SOC_{\min} c_V F} \quad (1)$$

The cell volumetric flow rate $Q_{cell}$ is a function of electrical density current $J$, membrane area $A_m$, flow factor $\alpha_Q$ that defines the operational range of cell volumetric flow rate (Tang *et al.* [9]), minimum state of charge $SOC_{min}$, vanadium molar concentration $c_V$ and, finally, Faraday constant $F$. In equation (1), the velocity inlet $v_{in}$ can be obtained from the number of membranes that compose the RFB ($n_m$), the number of inlet channels ($n_{ch}$) and the cross section area of the channels ($A_{ch}$). Besides $n_{ch}$ and $A_{ch}$ already reported in table 1, the other parameters needed in equation (1) are shown in detail in table 2.
As reported by Tang *et al.* [9], the flow factor $\alpha_Q$ can be chosen in the range of 1÷8. All the simulations have been performed with $\alpha_Q$ equal to 1. A pressure outlet condition is imposed for the outlet channels. Being the Reynolds number at inlet lower than 10, the fluid flow is assumed to be laminar.

**Table 2.** Values of the parameters adopted in equation 1.

| $n_m$ | $J$ [A m$^{-2}$] | $A_m$ [m$^2$] | $\alpha_Q$ | $SOC_{min}$ | $C_V$ [mol m$^{-3}$] | $F$ [C mol$^{-1}$] |
|---|---|---|---|---|---|---|
| 2 | 2000 | 0.0416 | 1 | 0.25 | 1600 | 96000 |

*3.1. Governing equations*
The porous media model can be used in many applications including flow through packed beds, filter papers, tube banks, felts, etc. In the present CFD simulations, the presence of the porous media is not physically represented, but it has been evaluated adding two source terms to the standard momentum equations: a viscous loss term and an inertial loss term. Only in these additional terms, the effect of the porous media have been considered. In fact, the porosity has not been taken into account in the convection and diffusion terms of transport equations. This numerical procedure is well-known and the fluid velocity obtained from these modified momentum equations is named superficial velocity, i.e. the velocity that the fluid would have if it flowed through the nominal cross section area of the porous media. There is a more accurate option called physical velocity method, where the true fluid velocity inside the porous media can be evaluated and the porosity can be considered inside the convection and diffusion terms, but no significant difference has been noted between the results of the two methods.
All the simulations have been performed with the superficial velocity method and fluid cells have been divided in two domains: the first one without the porous zone, i.e. the flow in the channels, and the second one with the porous zone, i.e. the flow in the carbon felt, where the additional terms have been calculated for a homogeneous porous media.
These momentum sources have been introduced as pressure gradient proportional to the fluid velocity:

$$\nabla p = -\left( \frac{\mu}{\alpha} v_i + \frac{1}{2} C_2 \rho |v| v_i \right) \quad (2)$$

As shown in equation (2), the coefficients of both terms are a function of transport properties of the fluid, i.e. density and dynamic viscosity, and geometrical characteristics of the porous media, i.e. permeability $\alpha$ and inertial loss coefficient $C_2$, that have been evaluated from the Ergun equation and Blake-Kozeny equations:

$$\alpha = \frac{d_e^2}{150} \frac{\varepsilon^3}{(1-\varepsilon)^2}; \; C_2 = \frac{3.5}{d_e} \frac{(1-\varepsilon)}{\varepsilon^3} \quad (3)$$

The geometrical characteristics reported above in equation 3 are functions of the media porosity $\epsilon$ and the hydraulic diameter $d_e$ of cylindrical fibers that compose the carbon felt. For all the simulations, the porosity and the diameter of fibers have been imposed, respectively, equal to 0.84 and $10^{-6}$ m.

It should be noted that, in the present work, the assumption of a thermal equilibrium between the porous media and the fluid flow has been considered and all the numerical simulations have been run excluding the energy equation.
As a first step, all the numerical simulations have been run considering the whole domain without the porous media to obtain an initial field flow and, in a second time, the porous zone has been enabled in the carbon felt domain. Finally, regarding the solution methods employed, a SIMPLE scheme has been used for pressure-velocity coupling, whereas a standard and second order upwind method have been imposed for the spatial discretization of pressure and momentum.

## 4. Results

A comparison of velocity fields, velocity distributions and pressure drop has been performed to highlight the different hydraulic performance of the four configurations. This method aims at evaluating the best configuration in terms of velocity field and pressure drop. All the results have been reported in terms of physical velocity $v_{ph}$ on the *x-y* plane, as defined in equation (4). The physical velocity has been calculated from the porosity $\epsilon$ and the superficial velocity $v$ obtained directly from the numerical simulations:

$$v_{ph} = \frac{\sqrt{v_x^2 + v_y^2}}{\varepsilon} \tag{4}$$

The velocity fields are reported in figure 2 showing the difference of the fluid flow behavior in each configuration at 50% of depth inside the carbon felt (the electrolyte enters at the bottom and exits from the top of figure).

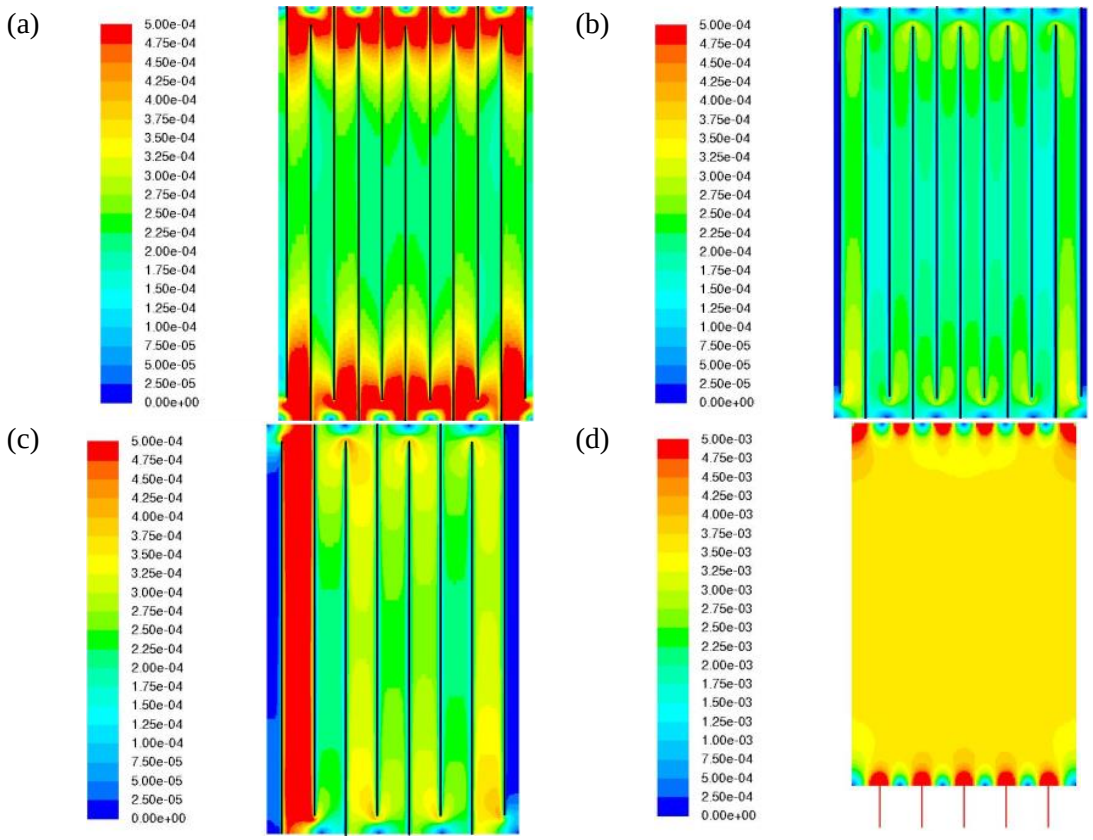


**Figure 2.** The velocity field ([m $s^{-1}$]) of the 5x6 1 mm h.d. (a), 5x6 2 mm h.d. (b), 4x4 2 mm h.d. (c) configuration with indirect feeding and the velocity field with direct feeding (d).

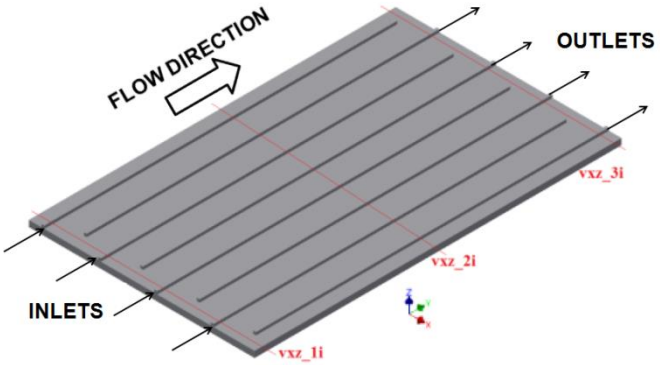


**Figure 3.** Red lines along which the velocity profiles are calculated. The index *i*, equal to 1, 2 or 3, is referred to 25%, 50%, 75% of depth inside the felt (configuration 3).

As depicted in figures 4-5, the planar velocity profiles along nine lines perpendicularly to the main flow direction (figure 3) have been calculated to investigate the velocity distribution inside the carbon felt. It should be noted that only the *x-y* velocity components have been considered at different depths inside the porous media (index *i*).
Beside the velocity trends, an investigation on velocity distributions has been performed to highlight the uniformity of the velocity field inside the felt. In all the configurations, it can be observed that the velocity profiles at lines *xz_1i* and *xz_3i* are affected by the channels inlets/outlets, while in correspondence of lines *xz_2i* the velocity trend is flatter, especially for the first and last configurations. It is worth noting that the velocities are reported at different depths inside the porous media (the index *i*, equal to 1, 2 or 3, is referred respectively to 25%, 50%, 75% of the depth inside the felt). A non-significant influence of depth on the velocity can be observed: it means that the distribution problem is restricted to the *x-y* plane and the investigation on planar velocity is thus justified.

### *4.1. Effect of hydraulic diameter*

Regarding the influence of the channel hydraulic diameter on the velocity field, a comparison of velocity profiles between the first and the second configuration can be considered. As mentioned above, the volumetric flow rate is the same for all numerical simulations, hence, for case 1, the velocity and pressure drop inside the channel are higher than those for case 2, due to a lower hydraulic diameter. In case 1, the electrolyte solution is mostly driven into the carbon felt and the velocity field is increased, as depicted in figure 2. Instead, for configuration 2, the fluid goes slower into the carbon felt creating stagnation zones below the channels and at lateral sides. The high velocity of case 1 causes a more uniform distribution of electrolyte along the lines *xz_2i*. This aspect is highlighted by the calculation of velocity distribution and it can be observed that, in the second case, the velocity values are more dispersed than those observed in the first case along the lines *xz_2i*.

### *4.2. Effect of number of inlet/outlet channels*

Concerning the influence of the number of channels on the velocity field, a comparison of velocity trends between the second and the third configuration can be considered. Two different behaviors can be observed:

- reducing the number of channels (case 3), the velocity profiles become flatter and the fluid goes through the felt with a longer path, increasing the pressure drop as compared to case 2. Furthermore, it can be observed that the velocity values in case 3 are closer to the mean value as compared to case 2 and thus the velocity field is more uniform.
- when the number of inlet channels is equal to the number of outlet channels (case 3), an asymmetric flow takes place and a maldistribution effect occurs from left to right, as depicted in figure 4. For the third case, this effect occurs because the fluid flowing inside the first inlet

channel on the left side is forced to go only through the outlet channel on the right, whereas the fluid flowing in the other inlet channels can go through its two neighbor outlet channels. For this reason, the electrolyte flow is higher on the left side as compared at the right side. This phenomenon does not occur in case 2, where the fluid in the first inlet channel can flow through the two neighbor outlet channels, providing a more uniform velocity field.

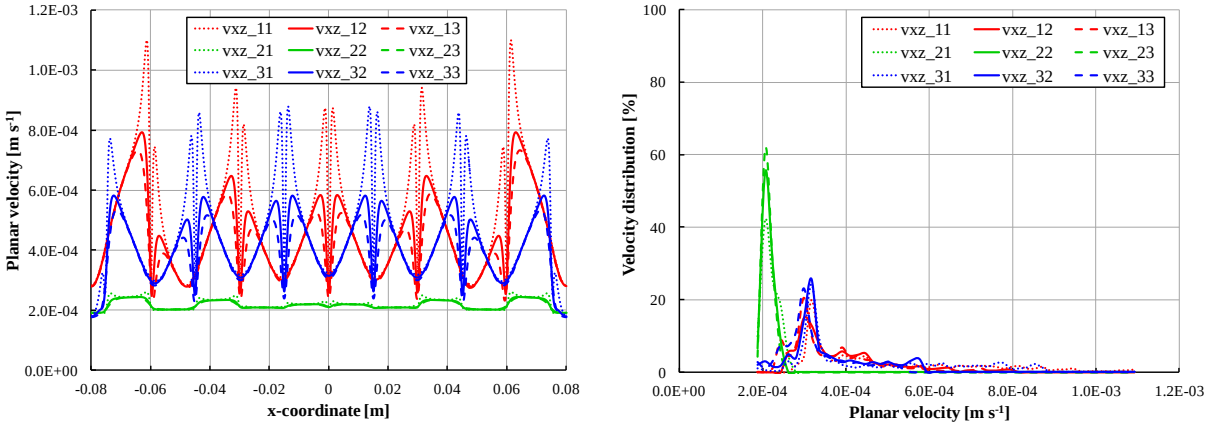


(a)

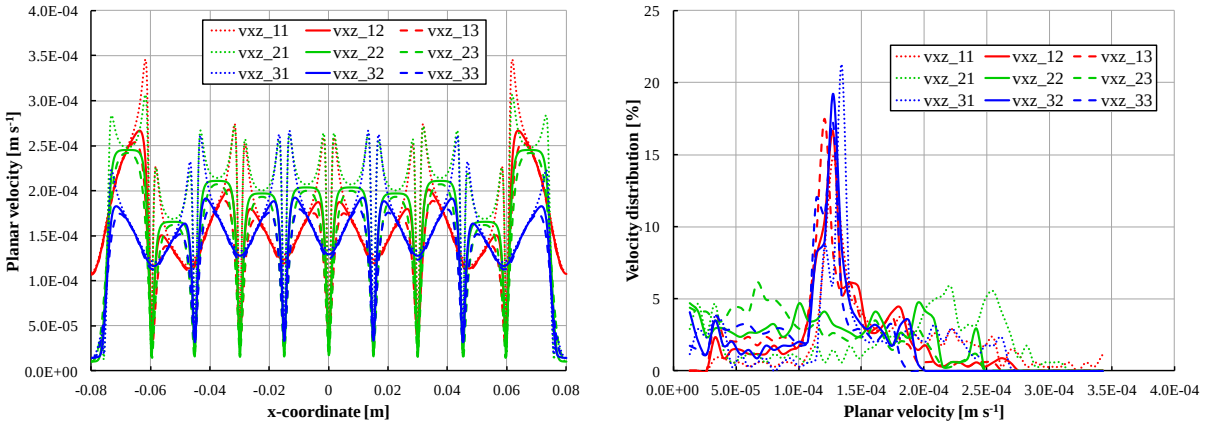


(b)

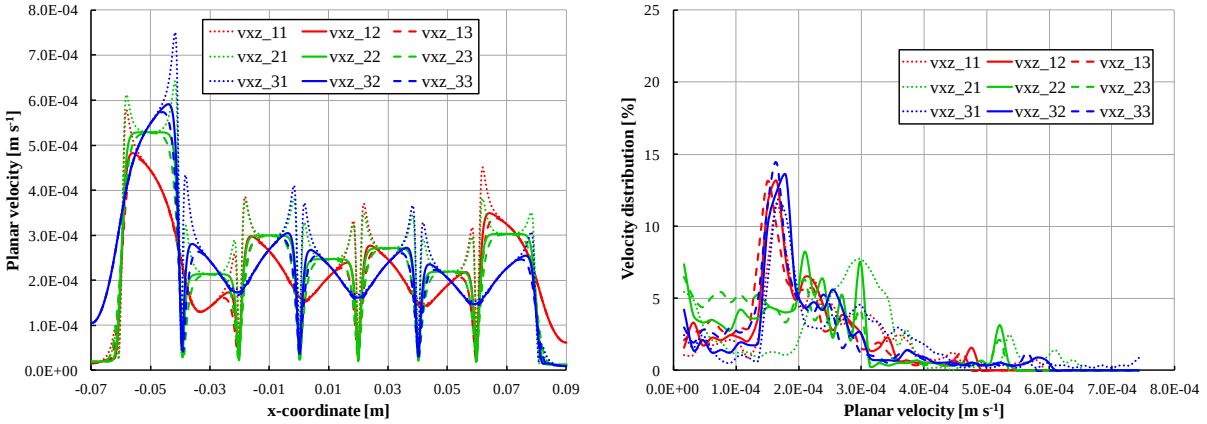


(c)

**Figure 4.** Planar velocity profiles calculated along the lines of figure 3 (left side) and velocity distribution (right side) for the 5x6 1 mm h.d. (a), 5x6 2 mm h.d. (b) 4x4 2 mm h.d. (c) configuration with indirect feeding.

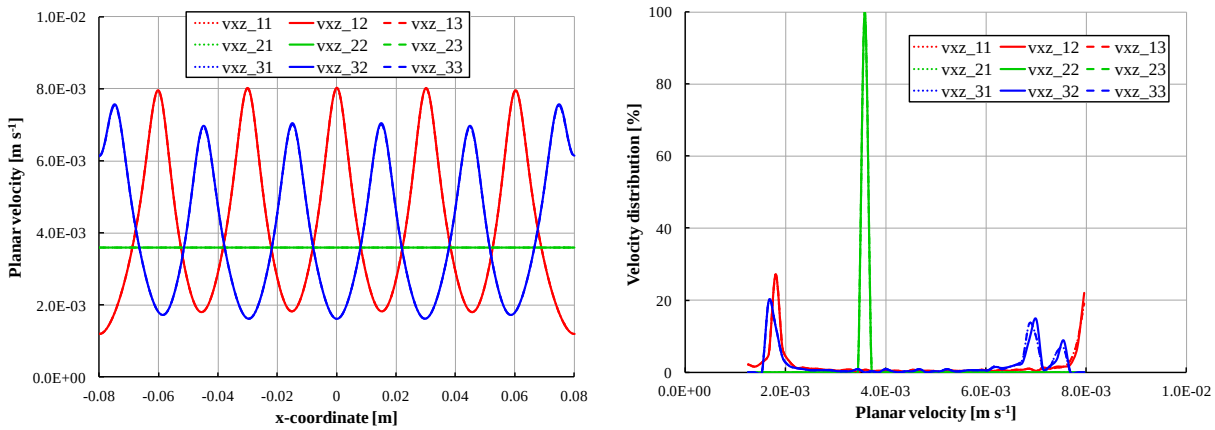


**Figure 5.** Planar velocity profiles calculated along the lines of figure 3 (left side) and velocity distribution (right side) for the configuration with direct feeding.

*4.3. Effect of feeding type*

With the aim to study the influence of feeding type on the velocity field, a comparison of velocity profiles between the first and the last configuration can be considered. It is important to notice that, in the case of a direct feeding, the velocity field is higher and more uniform as compared to the first configuration, as depicted in figures 4-5. However, using the direct feeding, the pressure drop is higher as compared to the configuration with indirect feeding.

Moreover, from figures 4(a)-5 along lines *xz_2i*, for both configurations, the velocities are close to the mean values and the velocity trends are similar. For this reason, it is very interesting to compare the four configurations taking into account the pressure drop. Beside the velocity trends along the different lines, the volume-weighted average of planar velocity inside the carbon felt has been calculated as reported in equation 5 to consider, at the same time, the effect of high velocity and stagnation zones.

$$v_{ph}\big|_V = \frac{1}{V}\int_V v_{ph}\,dV \tag{5}$$

**Table 3.** The volume-weighted average of physical planar velocity and pressure drop for the four configurations.

| Configuration | $v_{ph}\|_V$ [m s$^{-1}$] | $p_{in}$-$p_{out}$ [kPa] |
|---|---|---|
| **1** | 3.22E-04 | 10.61 |
| **2** | 1.98E-04 | 1.40 |
| **3** | 2.71E-04 | 2.30 |
| **4** | 3.69E-03 | 210.50 |

As reported in table 3, the first configuration is the one that assures the highest volume-weighted average velocity for indirect feeding, whereas considering all the configurations, the case with the highest value of $v_{ph}|_V$ is the case number 4.

*4.4. Pressure Drop*

In the present section, the pressure drop has been calculated in order to evaluate the performance of the RFB cell in terms of pumping consumption. For the estimation of pressure drop, the area-weighted average of static pressure has been calculated at the inlet and outlet of channels for each configuration.

The relationship between the pressure drop and the velocity distribution can be observed in table 3. Indeed, the first and the fourth configurations present the highest value of pressure drop. The pressure

drop in case 1 and 4 are higher, respectively, up to 7 and 150 times as compared to the configuration 2 that presents the worst distribution. The second and the third case display the lowest pressure drop but both configurations have many stagnation zones and the third one is affected by maldistribution problems. In conclusion, a good compromise would be the first solution since the velocity is high enough to avoid the presence of stagnation zones and to guarantee a velocity field almost uniform. In addition, the total pressure drop of the first case are limited as compared to the fourth case.

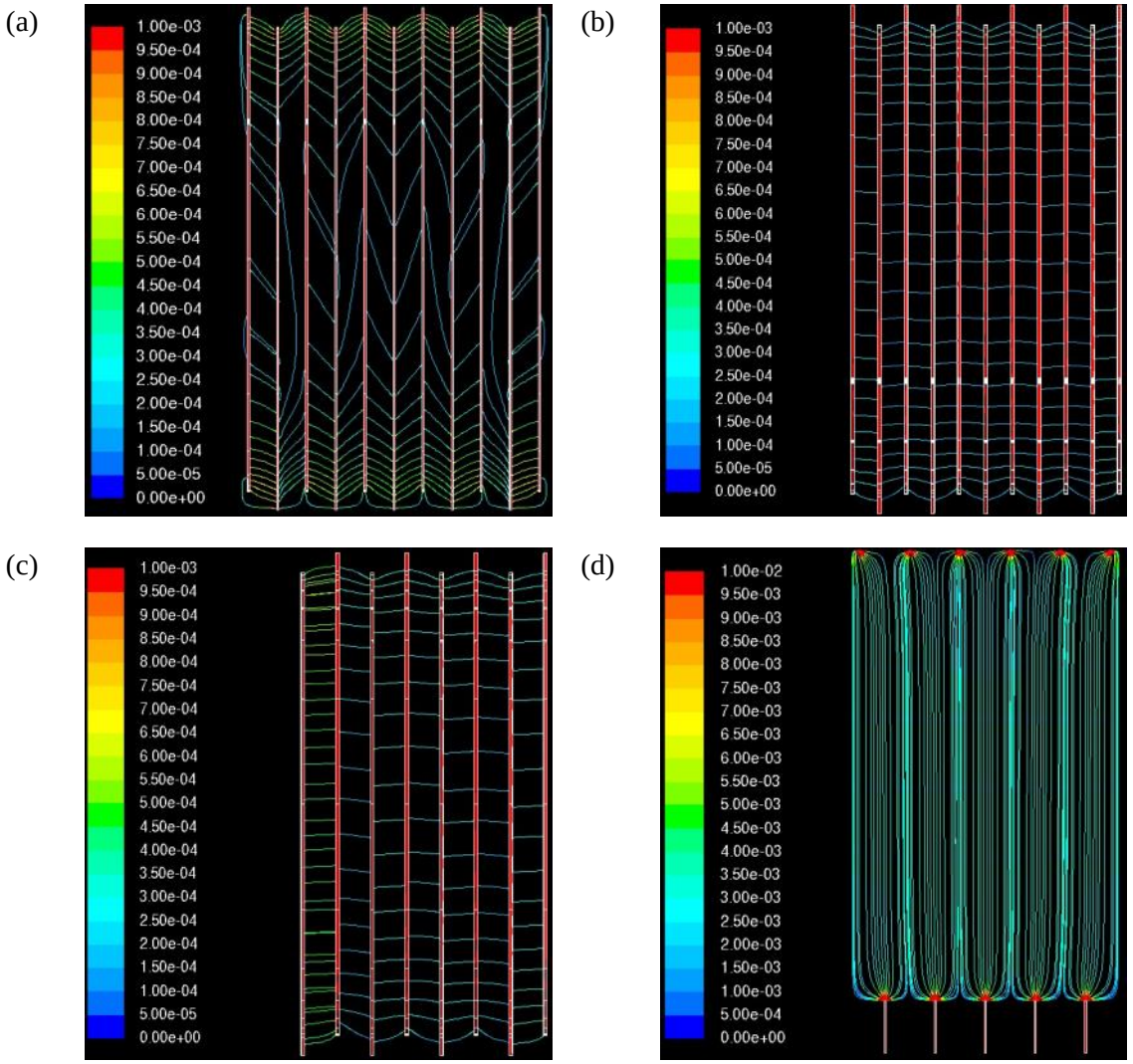


**Figure 6.** Planar velocity streamlines in [m $s^{-1}$] for the three configurations with indirect feeding (5x6 1 mm h.d. (a), 5x6 2 mm h.d. (b), 4x4 2 mm h.d. (c)) and for the one with direct feeding (d).

### *4.5. Streamlines*

As mentioned above, to improve the performance of RFB it is fundamental to guarantee:

- a good-distribution of the electrolyte in terms of velocity, avoiding stagnation or dry zones inside the porous felt;
- low pressure drop and low pumping consumption.

For this purpose, the importance of the fluid path inside the porous media must be underlined. In fact, if the fluid has a long path inside the porous felt, the probability of electrochemical reaction occurring is higher and the RFB performance can be improved.

From this point of view, the direct feeding of electrolyte inside the carbon felt is the best configuration since the fluid is constrained to cross the whole felt as compared to the indirect feeding. As depicted in figure 6, it can be observed that, for the second and third configuration, the electrolyte solution flows from inlet to outlet channels through a very short path as compared to the first case where its path inside the felt becomes longer.

## 5. Conclusions

In this paper, four different geometrical configurations have been considered to evaluate the influence of the electrolyte solution distribution system (inlet/outlet number of channels, channels hydraulic diameter, feeding mode) on velocity field and pressure drop inside a RFB cell. Different parameters have been considered to assess the RFB fluid dynamic performance: planar velocity profiles, pressure drop and velocity streamlines.
The following conclusions can be drawn:

- the first and the fourth configuration present an almost uniform velocity field as compared to the second and third case where stagnation zones have been found below the channels and at the lateral sides of the carbon felt;
- a long fluid path inside the carbon felt can improve the performance of the RFB in terms of electrochemical reactions. For this reason, the second and the third case are the worst configurations due to very short fluid path inside the porous zone;
- the fourth case with direct feeding has the highest pressure drop, up to 150 times higher than the second case. Considering both electrolyte solution distribution and pumping power, the first case results as the best choice according to the present simulations.

## Acknowledgements

This work was supported by the University of Padova under the MAESTRA 2011 strategic project.

## 6. References

[1] Alotto P, Guarnieri M and Moro F 2014 Redox flow batteries for the storage of renewable energy: A review *Renew. Sust. Energy Rev.* **29**, 325-35
[2] Cunha A, Martins J, Rodrigues N and Brito F P 2015 Vanadium redox flow batteries: A technology review *Int. J. Energy Res.* **39**, 889-918
[3] Weber A Z, Mench M M, Meyers J P, Ross P N, Gostick J T and Liu Q 2011 Redox flow batteries: A review *J. Appl. Electrochem.* **41**, 1137-64
[4] Ponce D L C, Frias Ferrer A, Gonzalez Garcia J, Szanto D A and Walsh F C 2006 Redox flow cells for energy conversion *J. Power Sources* **160**, 716-32
[5] Wei Z, Zhao J, Skyllas Kazacos M and Xiong B 2014 Dynamic thermal-hydraulic modeling and stack flow pattern analysis for all-vanadium redox flow battery *J. Power Sources* **260**, 89-99
[6] Xu Q, Zhao T S and Leung P K, 2013 Numerical investigations of flow field designs for vanadium redox flow batteries *Appl. Energy* **105**, 47-56
[7] Blanc C and Rufer A 2008 Multiphysics and energetic modeling of a vanadium redox flow battery, 696-701
[8] Tang Z, Aaron D S, Papandrew A B and Zawodzinski Jr T A 2012b Monitoring the state of charge of operating vanadium redox flow batteries **41**, 1-9
[9] Tang A, Ting S, Bao J and Skyllas-Kazacos M 2012a Thermal modelling and simulation of the all-vanadium redox flow battery J. Power Sources **203**, 165-76